Aalborg Universitet

AALBORG UNIVERSITY
DENMARK

Fault Coordination Control for Converter-interfaced Sources Compatible with Differential Protection during Asymmetrical Faults

Yang, Zhe; Liao, Wenlong; Bak, Claus Leth; Chen, Zhe

Published in:
Energy Reports

DOI (link to publication from Publisher):
10.1016/j.egyr.2022.08.045

Creative Commons License
CC BY-NC-ND 4.0

Publication date:
2022

Document Version
Publisher's PDF, also known as Version of record

Link to publication from Aalborg University

Citation for published version (APA):
Yang, Z., Liao, W., Bak, C. L., & Chen, Z. (2022). Fault Coordination Control for Converter-interfaced Sources Compatible with Differential Protection during Asymmetrical Faults. *Energy Reports*, *8*(Suppl. 13), 249-258. https://doi.org/10.1016/j.egyr.2022.08.045

General rights
Copyright and moral rights for the publications made accessible in the public portal are retained by the authors and/or other copyright owners and it is a condition of accessing publications that users recognise and abide by the legal requirements associated with these rights.

- Users may download and print one copy of any publication from the public portal for the purpose of private study or research.
- You may not further distribute the material or use it for any profit-making activity or commercial gain
- You may freely distribute the URL identifying the publication in the public portal -

Take down policy
If you believe that this document breaches copyright please contact us at vbn@aub.aau.dk providing details, and we will remove access to the work immediately and investigate your claim.

Available online at www.sciencedirect.com
ScienceDirect
Energy Reports 8 (2022) 249–258
www.elsevier.com/locate/egyr

The 5th International Conference on Electrical Engineering and Green Energy, CEEGE 2022, 8–11 June, Berlin, Germany

Fault coordination control for converter-interfaced sources compatible with differential protection during asymmetrical faults

Zhe Yang, Wenlong Liao*, Claus Leth Bak, Zhe Chen

AAU Energy, Aalborg University, Aalborg, 9220, Denmark

Received 15 July 2022; accepted 5 August 2022
Available online xxxx

Abstract

Converter-interfaced renewable energy sources (CIRESs) may have a different fault current angle with synchronous generators (SGs), so the large angle difference on both sides will cause low sensitivity or failure for traditional proportional braking differential protection. So as to cope with this issue, a new fault control strategy is put forward. By analyzing the phasor diagram during asymmetric faults, a reasonable phase angle of the CIRES fault current is determined to reduce the angle difference below 60°, and corresponding current references of the controller are calculated. In this way, the proposed method can make CIRESs compatible with differential protection, so it is economical since the protection device is not necessary to be updated. In addition, it also shows good performance for different fault points, high-resistance faults and different power factors before the fault. Moreover, typical fault ride through (FRT) conditions including fault current restriction and reactive power support are still being satisfied while the controller structure does not require to be altered. Simulation results in PSCAD validate the proposed approach can be used for different fault scenarios.
© 2022 The Author(s). Published by Elsevier Ltd. This is an open access article under the CC BY-NC-ND license (http://creativecommons.org/licenses/by-nc-nd/4.0/).

Peer-review under responsibility of the scientific committee of the 5th International Conference on Electrical Engineering and Green Energy, CEEGE, 2022.

Keywords: Fault control; Fault ride through; Pilot protection; Renewable energy sources

1. Introduction

With the increase in the installed capacity and the electrical production for renewable energy sources (RESs), RESs will have an evident impact on the protection system [1,2]. Unlike synchronous generators (SGs), converter-interfaced RESs (CIRESs) are integrated into the power system by full-power inverters [3], so their distinct fault features will be harmful for the performance of proportional braking differential protection [4,5].

Differential protection is often deployed on the transmission line and can cut off the line within a short time [6]. At present, many researchers focus more on the impact of doubly-fed induction generators (DFIGs) on differential protection [7–9]. Authors in [7] pointed out that the fault current from DFIGs did not affect the performance of differential protection, but the influence of the rotor-speed-frequency fault current is not considered when the

* Corresponding author.
E-mail address: weli@energy.aau.dk (W. Liao).

https://doi.org/10.1016/j.egyr.2022.08.045
2352-4847/© 2022 The Author(s). Published by Elsevier Ltd. This is an open access article under the CC BY-NC-ND license (http://creativecommons.org/licenses/by-nc-nd/4.0/).

Peer-review under responsibility of the scientific committee of the 5th International Conference on Electrical Engineering and Green Energy, CEEGE, 2022.

Crowbar device is activated. The non-fundamental-frequency current could cause the fluctuation of the extracted phase angle, so differential protection will misoperate [8,9]. Additionally, some researches are also related to the impact of CIRESs on differential protection. It may fail to be activated for phase-to-phase faults if the short-circuit capacity of CIRESs is near to that of the connected grid because the phase angle difference on both ends will be larger than 90° such that the operating current will be lower than the restraint current under some fault ride through (FRT) strategies [10]. In addition, the operating current would be basically equal to the braking current when the integrated capacity of CIRESs is small, which leads to low sensitivity of differential protection [11]. Moreover, the small fault current from CIRESs may not activate the starting element of differential protection [12].

Many new pilot protection methods have been proposed to cope with this problem. A concept of differential impedance was put forward in [13], and its amplitude feature was applied for identifying the fault zone, but the data must be transmitted synchronously. Another differential relay was designed using the differential impedance and restraint impedance, but its sensitivity will be reduced evidently for high resistance faults [14]. Since the CIRES fault current is usually smaller than that of SGs, so a current amplitude ratio-based pilot protection was proposed in [15]. Some scholars introduced the parameter identification methods into protection field. The differential current would be equal to the derivative value of the differential voltage multiplied by the line capacitance for external faults, but it was not established for internal faults, so this difference was utilized to form a novel protection scheme [16]. However, the derivative term is influenced by high-order components, thus it sometimes cannot show good performance. In addition, transient currents on both terminals are greatly diverse, thus numerous mathematical methods are applied to measure the current similarity with a time window of data [17–19]. The authors in [17] used Pearson coefficient to detect the fault. Similarly, a method utilizing Cosine similarity was proposed in [18] with faster speed. However, the above methods will fail to operate when the fault current from RESs is equal to 0. For this issue, another approach utilizing Spearman's correlation factor was put forward in [19]. These methods are effective for the situation with RES integration, but they all need to update the protection devices in the vicinity of RESs. In recent years, active control-based methods have attracted attention [20], but the related control scheme is not reported to maintain the correct operation for traditional differential protection.

A new fault coordinative control scheme is proposed to make traditional differential protection operate correctly, and it has the following contributions: (1) the proposed method can make CIRESs compatible with differential protection. (2) Typical FRT conditions such as reactive current injection and fault current limiting can be achieved. (3) Only the local measured data are used while the typical controller structure is not necessary to be revised.

2. The tested system with CIRESs

CIRESs are connected to the collection line by the step-up transformer. After that, the produced power is transmitted to the remote end by the high-voltage transmission line, as shown in Fig. 1.

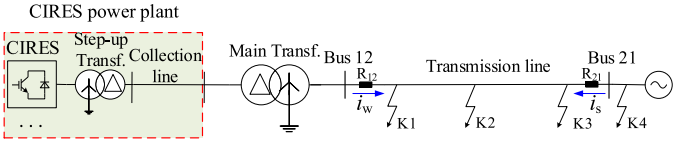

Fig. 1. The studied topology in PSCAD.

The rated power of the CIRES power plant is 500 MW, and the transmission line is 40 km with a voltage level of 220 kV. The positive-sequence impedance of the line is 0.043+j0.432 Ω/km, and the grid impedance is equal to 0.4+j12.568 Ω, so the integrated CIRES capacity equals one-quarter of the short-circuit capacity of the connected grid. Three internal fault points, K1, K2, and K3 are respectively located at 0 km, 20 km, 40 km of the line, and an external fault K4 is set to the right side of Bus 21. Differential relay is deployed at two ends of the overhead line to detect all the faults between Bus 12 and Bus 12. Letters A, B and C mean different faulty phases while G denotes the phase to ground.

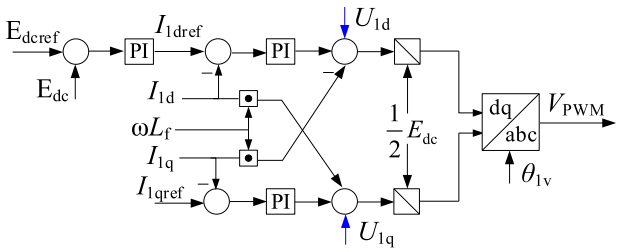

Fig. 2. The control structure of CIRESs. (For interpretation of the references to color in this figure legend, the reader is referred to the web version of this article.)

3. Problem statement

3.1. Fault current of CIRESs

The controller of CIRESs is based on decoupled current control (DCC) with the voltage vector oriented at the positive-sequence d axis [21], as depicted in Fig. 2.

In the figure, the constant DC control is utilized to produce the d-axis current reference, and the q-axis current reference value is taken as 0 during normal operation, so CIRESs usually work at the unity power factor. When a fault appears, the outer voltage loop will be cut off, and current references are given according to the specific grid codes. At this time, since the grid voltage is added in the current controller (marked in blue), thus the fault current from CIRESs is always symmetric for different fault types [20]. The phase-A current expression of CIRESs can be written as:

$$i_{\text{fa\_CIRES}}(t) = \sqrt{I_{\text{1dref}}^2 + I_{\text{1qref}}^2}\cos\left(\omega_1 t + \theta_{1v} + \arctan\left(\frac{I_{\text{1qref}}}{I_{\text{1dref}}}\right)\right) \tag{1}$$

where ω_1 and θ_{1v} are the angular velocity and the initial phase angle obtained from the phase-locked loop, t denotes the initial fault time. Additionally, the phase-B and Phase-C fault currents will lag or lead by 120°.

As seen from (1), the CIRES current angle is strongly related to current references, so the phase angle will be very different for different grid codes.

3.2. Adaptive analysis for phase-to-phase faults

For traditional transmission lines with two-end sources, the fault current angle on both ends is basically the same for inside-of-zone faults, yet reverse for outside-of-zone faults. Therefore, the operating current in (2) will be much higher than the braking current for inside-of-zone faults, and the conclusion is inverse for external faults.

$$\begin{cases} I_{\text{op}} \geq I_{\text{op0}}, \text{and } I_{\text{op}} \geq k_1 I_{\text{res}} \\ I_{\text{op}} = \left|\dot{I}_{\text{S}} + \dot{I}_{\text{W}}\right|, I_{\text{res}} = \left|\dot{I}_{\text{S}} - \dot{I}_{\text{W}}\right| \end{cases} \tag{2}$$

where I_{op} denotes the operating current, I_{res} denotes the braking current, and I_{op0} denotes the starting current. $\dot{I}_{\text{S}}$ and $\dot{I}_{\text{W}}$ are respectively current phasors measured at R_{12} and R_{21}. k is the braking factor that is taken as 0.8 in this paper.

When a BC fault appears at the line, the current phasors will satisfy the following relationship:

$$\dot{I}_{\text{WB}} + \dot{I}_{\text{WC}} + \dot{I}_{\text{SB}} + \dot{I}_{\text{SC}} = 0 \tag{3}$$

Where subscripts W and S denote the electric components measured at R_{12} and R_{21}.

Since CIRESs always output the three-phase symmetric fault current, (3) can be simplified as:

$$\dot{I}_{\text{SB}} + \dot{I}_{\text{SC}} = \dot{I}_{\text{WA}} \tag{4}$$

In addition, the phase angle difference between $\dot{I}_{\text{SB}}$ and $\dot{I}_{\text{SC}}$ will be slightly smaller than 180° [10]. Therefore, the current phasor diagram can be depicted in Fig. 3 when CIRESs are connected.

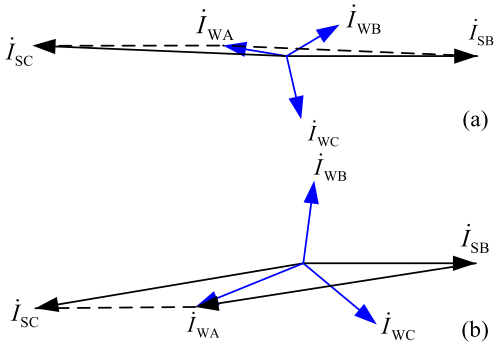

Fig. 3. Current phasor diagram.

When the phase angle of $\dot{I}_{SC}$ leads that of $\dot{I}_{SB}$, the angle difference between $\dot{I}_{SC}$ and $\dot{I}_{WC}$ will be larger than 90° and smaller than 120°. At this time, the operating current will be lower compared with the braking current for phase-C. In addition, the angle difference will be larger than 120° when the phase angle of $\dot{I}_{SC}$ lags that of $\dot{I}_{SB}$, so differential protection will be more prone to misoperation.

3.3. Adaptive analysis for grounding faults

For grounding faults, a large zero-sequence current will flow through the line. In this situation, the angle difference on two terminals will be reduced hugely. Therefore, differential relay can usually operate.

In summary, differential relay may misoperate for line-to-line faults, but it can operate correctly for grounding faults.

4. New control scheme

Combined with sequence current phasor diagrams, a reasonable fault current angle of CIRESs is found to make differential relays operate correctly. The related current references are calculated considering FRT conditions.

4.1. Relationship between current references

When a BC fault occurs, the sequence network diagram is depicted in Fig. 4.

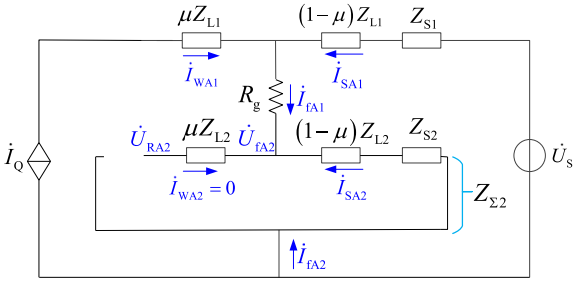

Fig. 4. Sequence network diagram when a BC fault appears.

In the figure, subscripts 1, 2 denote positive and negative-sequence components, respectively. Z_S and Z_L represent the grid impedance and the line impedance. CIRESs are equivalent to a controllable current source, and the grid is modeled as the constant voltage source with an impedance. R_g denotes the fault resistance. According to sequence boundary conditions for phase-to-phase faults, there is:

$$\begin{cases} \dot{I}_{fA1} = -\dot{I}_{fA2} \\ \dot{I}_{WA1} + \dot{I}_{SA1} = \dot{I}_{fA1} \end{cases} \tag{5}$$

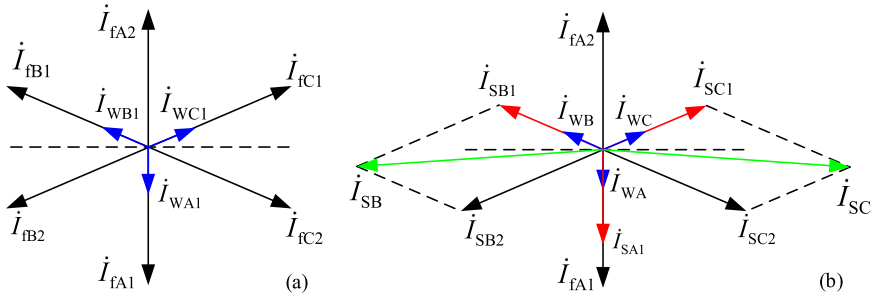

Fig. 5. Sequence current phasor diagrams for phase-to-phase faults. (For interpretation of the references to color in this figure legend, the reader is referred to the web version of this article.)

Based on this, the sequence current phasor diagram can be depicted in Fig. 5(a). When the phase angle of $\dot{I}_{\mathrm{WA}}$ is controlled to be equal to that of $\dot{I}_{\mathrm{fA1}}$ (blue arrows in Fig. 5(a)), the angle of $\dot{I}_{\mathrm{SA1}}$ will be also equal to that of $\dot{I}_{\mathrm{fA1}}$ according to (4). In this situation, current angles on two terminals are depicted in Fig. 5(b). The phase angle difference between $\dot{I}_{\mathrm{SB}}$ and $\dot{I}_{\mathrm{WB}}$ will be equal to the angle difference between $\dot{I}_{\mathrm{SC}}$ and $\dot{I}_{\mathrm{WC}}$, and both will be smaller than 60°. In this way, the operating current is higher than the braking current, so differential relays will operate correctly.

Since the phase angle of $\dot{I}_{\mathrm{fA1}}$ cannot be measured by R_{12} directly, a method to detect this phase angle needs to be proposed. There is no negative-sequence current from CIRESs, so (6) can yield:

$$\begin{cases} \dot{I}_{SA2} = \dot{I}_{\mathrm{fA2}} \\ \dot{U}_{\mathrm{RA2}} = \dot{U}_{\mathrm{fA2}} = -\dot{I}_{\mathrm{fA2}} \left((1-\mu) Z_{L2} + Z_{S2} \right) \end{cases} \tag{6}$$

where $\dot{U}_{\mathrm{RA2}}$ is the negative-sequence voltage detected by R_{12}.

As illustrated in (5), the phase angle of $\dot{I}_{\mathrm{fA2}}$ can be calculated by $\dot{U}_{\mathrm{RA2}}$ because the impedance angle of (1-μ)Z_{L2}+Z_{S2} can be considered to be a constant value. In the studied model, the impedance angle is 84.29°. Therefore, (6) can yield:

$$\angle \dot{I}_{\mathrm{SA2}} = \angle \dot{U}_{\mathrm{RA2}} - \angle \left((1-\mu) Z_{L2} + Z_{S2} \right) + 180^{\circ} \tag{7}$$

where $\angle$ denote the angle of a phasor.

After that, the required phase angle of $\dot{I}_{\mathrm{WA1}}$ in Fig. 5(a) can be calculated as:

$$\angle \dot{I}_{WA1} = \angle \dot{I}_{fA1} = \angle \dot{I}_{fA2} - 180^{\circ} \tag{8}$$

In this way, the phase angle of $\dot{I}_{\mathrm{WA1}}$ can be determined. To make CIRESs output this fault current angle, the first condition for current references of the controller can be obtained using (1):

$$I_{\mathrm{1dref}} = \frac{I_{\mathrm{1qref}}}{\tan(\angle \dot{I}_{\mathrm{WA1}} - \theta_{1v} - 90^{\circ})} \tag{9}$$

The q-axis current I_{1qref} will be given by the specific grid code. This will be discussed in the next section.

4.2. Reactive current injection

The typical grid code about the reactive current injection is shown in Fig. 6, and I_{1qref} will be given according to voltage sags [5].

After I_{1qref} is decided, the corresponding I_{1dref} can be obtained by (9). The above process does not refer to the current limiting, so current references need to be adjusted as follows:

$$\begin{cases} I'_{\mathrm{1dref}} = {}^{I_{\mathrm{1dref}}}/_{M} \\ I'_{\mathrm{1qref}} = {}^{I_{\mathrm{1qref}}}/_{M} \end{cases}, \; M = \max\left(1, \frac{\sqrt{I_{\mathrm{1dref}}^2 + I_{\mathrm{1qref}}^2}}{\lambda}\right) \tag{10}$$

where λ denotes the current restriction value, which can be taken as 1.2 in this paper.

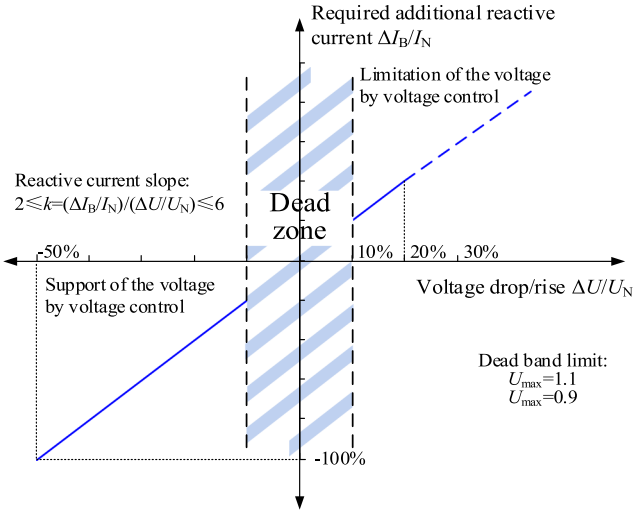

Fig. 6. A typical grid code about the reactive current injection.

When current references are given according to the above calculation results, the phase angle difference on both sides will be smaller than 60° such that differential protection can operate correctly.

5. Simulation analysis

This part will do the related simulation analysis to validate the existing problems of differential protection and the effectiveness of the proposed method. All the faults appear at 0.6 s, and CIRESs operate at the unity power factor on normal operation without the special statement.

5.1. Adaptive problem

For the traditional FRT strategy, I_{1dref} will be equal to $\sqrt{\eta^2 - I_{1qref}^2}$. In this situation, the phase angle difference between two terminals and the related values measured by differential relay are depicted in Fig. 7 for a BC fault at K1.

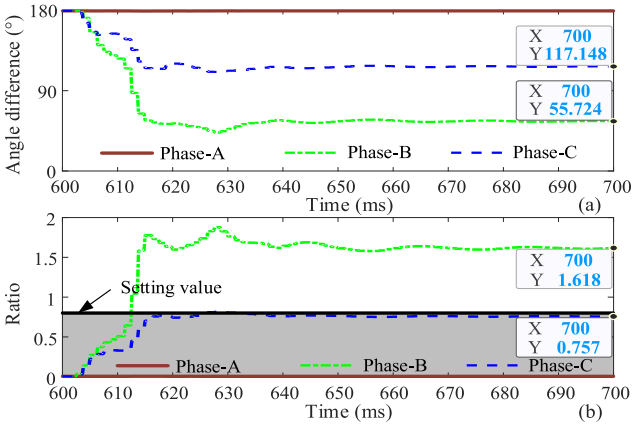

Fig. 7. Components detected by differential protection for the traditional FRT. (a) Angle difference, (b) ratio.

The angle difference in Fig. 7(a) for phase-C equals 117.148°, and it is 55.724° for phase-B, which is corresponding to the situation in Fig. 3(a). At this time, the differential relay for phase-C will fail to operate,

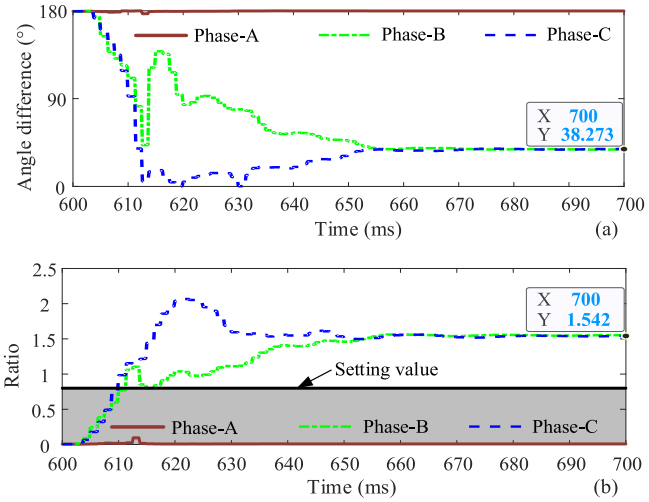

Fig. 8. Components detected by differential protection for the proposed control method. (a) Angle difference, (b) ratio.

as shown in Fig. 7(b). So as to improve the sensitivity of this differential relay, a new fault coordinative control strategy is proposed.

5.2. *Different fault points*

In the same fault conditions, the angle difference and the ratio of the operating current to the braking current have been illustrated in Fig. 8 when CIRESs adopt the proposed control strategy.

As known from Fig. 8(a), the angle errors are basically equal to 38.273° for phase-B and phase-C, and both are smaller than 60°, which are consistent with the analysis in Fig. 5(b). Under this circumstance, the ratios for phase-B and phase-C will be high than the threshold value, so differential relay can operate correctly.

For external faults, the angle difference between two terminals always approach 180° for different control strategies due to Kirchhoff's current law. To confirm this point, the measured components from this differential relays are depicted in Fig. 9 for a BC fault at K4.

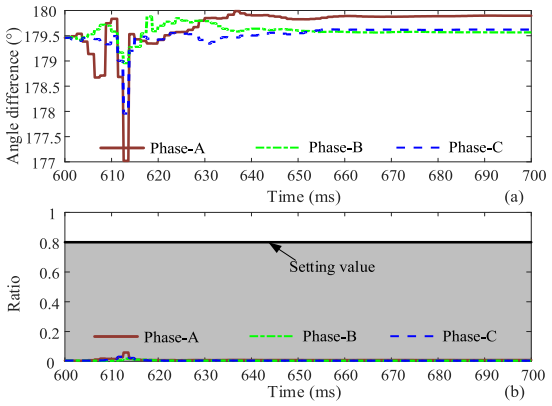

Fig. 9. Components detected by differential protection for external faults. (a) Angle difference, (b) ratio.

All the angle differences for three phases in Fig. 9(a) are close to 180°, so the ratios will be lower than the setting value such that differential relays can be blocked reliably, as shown in Fig. 9(b).

For all the fault points, the angle difference, and ratios measured by differential relays for BC faults will be summarized in Table 1. All the values are taken from 100 ms after the failure time.

Table 1. Ratios of differential protection under different fault points.

Fault location		A	B	C
K1	Difference	179.871	37.987	38.273
	Ratio	0.008	1.551	1.542
K2	Difference	179.867	35.336	35.398
	Ratio	0.008	1.358	1.352
K3	Difference	179.865	32.967	32.869
	Ratio	0.009	1.192	1.191
K4	Difference	179.897	179.567	179.621
	Ratio	0.009	0.004	0.004

As shown in Table 1, the ratios for two faulty phases are basically equal, and higher than the setting value because both angle differences are the same and lower than 60°. In addition, the ratios for external faults will be lower than the setting value. The results of these simulations are in line with the theoretical analysis.

5.3. Different fault resistances

This part will analyze the impact of the fault resistance on this new control method. When the fault resistances are taken as 50 Ω and 100 Ω, the performance of differential protection is given in Fig. 10 for a BC fault at K2.

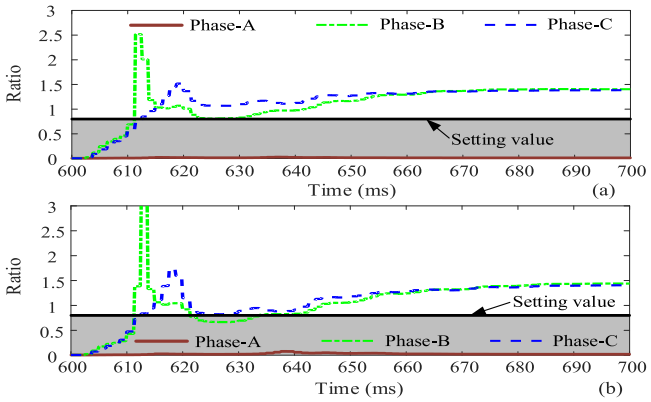

Fig. 10. Performance of differential protection for different fault resistances. (a) 50 Ω, (b) 100 Ω.

It can be known from Fig. 10(a) and (b) that the proposed control method is still effective for the case with 50 Ω and 100 Ω of fault resistances. The ratios for faulty phases are always higher than the setting value, and it is lower than the setting value for non-faulty phases, so differential protection can operate correctly.

5.4. Different power factors before the fault

In this section, the influence of different power factors before the fault on the proposed control scheme will be discussed. When power factors are respectively set to 0.9 and 0.95, and a BC fault appears at K3, the ratios detected by differential relays is illustrated in Fig. 11.

Compared with Fig, 11 (a) and Fig. 11(b), different power factors have a certain impact on the transient state (the part inside the oval) because they determine the initial state of the system. However, the ratios for faulty phases will be equal in both cases at the steady state, so this new control strategy can be applicable for various power factors.

6. Conclusion

The big phase angle difference between two terminals will bring about the failure of traditional differential relays for phase-to-phase faults. Simulation results validate this point combined with traditional FRT strategies.

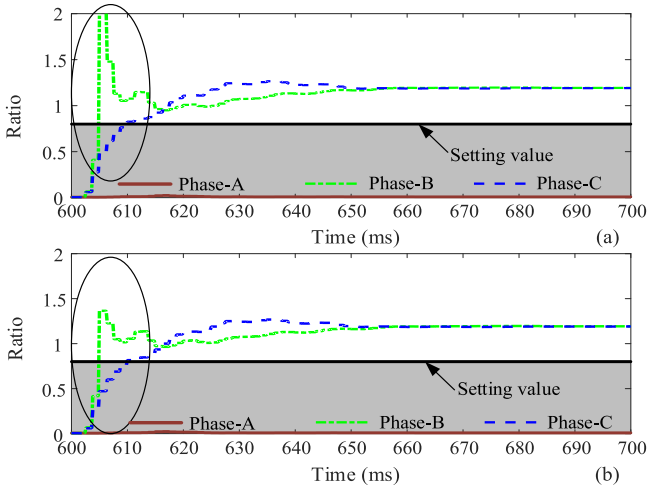

Fig. 11. Performance of differential protection for different power factors before the fault. (a) 0.9, (b) 0.95.

A new fault coordinative control scheme is presented to maintain the performance of differential relays for the line with CIRESs. Through analyzing the current phasor diagram, a reasonable CIRES fault current angle is determined. After that, corresponding current references are calculated considering typical FRT requirements. In this way, CIRESs can be compatible with differential protection. Besides that, the proposed control method is effective for different fault locations, fault resistances and power factors before the fault. In addition, only local measured data is used, and the typical controller structure is not necessary to be altered. PSCAD simulation confirms the proposed scheme

Declaration of competing interest

The authors declare that they have no known competing financial interests or personal relationships that could have appeared to influence the work reported in this paper.

Data availability

The data that has been used is confidential.

Acknowledgment

This work was supported by the China Scholarship Council (CSC).

References

[1] Bozalakov DV, Vandoorn TL, et al. Damping-based droop control strategy allowing an increased penetration of renewable energy resources in low-voltage grids. IEEE Trans Power Deliv 2016;31(4):1447–55.
[2] Fang Y, Jia K, Yang Z, Li Y, Bi T. Impact of inverter-interfaced renewable energy generators on distance protection and an improved scheme. IEEE Trans Ind Electron 2019;66(9):7078–88.
[3] Jia J, Yang G, Nielsen AH, Gevorgian V. Investigation on the combined effect of VSC-based sources and synchronous condensers under grid unbalanced faults. IEEE Trans Power Deliv 2019;34(5):1898–908.
[4] Telukunta V, Pradhan J, Agrawal A, Singh M, Srivani SG. Protection challenges under bulk penetration of renewable energy resources in power systems: A review. CSEE J Power Energy Syst 2017;3(4):365–79.
[5] Hooshyar A, Iravani R. Microgrid protection. Proc IEEE 2017;105(7):1332–53.
[6] Liu S, Zhang LL, Fu C, Jiang L. A new two-port network model-based pilot protection for AC transmission lines. IEEE Trans Power Deliv 2020;35(2):473–82.
[7] Li G, et al. DFIG-based wind farm electromagnetic dynamic model and impact on protection relay of transmission network. In: 2011 international conference on advanced power system automation and protection. 2011, p. 694–8.
[8] Hooshyar A, Azzouz MA, El-Saadany EF. Three-phase fault direction identification for distribution systems with DFIG-based wind DG. IEEE Trans Sustain Energy 2014;5(3):747–56.

[9] Hooshyar A, Azzouz MA, El-Saadany EF. Distance protection of lines connected to induction generator-based wind farms during balanced faults. IEEE Trans Sustain Energy 2014;5(4):1193–203.
[10] Li Y, Jia K, Bi T, Yan R, Li W, Liu B. Analysis of line current differential protection considering inverter-interfaced renewable energy power plants. In: 2017 IEEE PES innovative smart grid technologies conference europe (ISGT-Europe). 2017, p. 1–6.
[11] Dambhare S, Soman SA, Chandorkar MC. Adaptive current differential protection schemes for transmission-line protection. IEEE Trans Power Deliv 2009;24(4):1832–41.
[12] Yang G, et al. The influences and countermeasures of wind farm access to transmission line differential protection. In: 2012 IEEE power electronics and machines in wind applications. 2012, p. 1–4.
[13] Bolandi TG, Seyedi H, Hashemi SM, Nezhad PS. Impedance-differential protection: A new approach to transmission-line pilot protection. IEEE Trans Power Deliv 2015;30(6):2510–8.
[14] Chen G, Liu Y, Yang Q. An impedance-based protection principle for active distribution network. In: 2018 China international conference on electricity distribution (CICED), Tianjin. 2018, p. 1241–5.
[15] Jia K, et al. Amplitude comparison based pilot protection for renewable power teed line, CSEE J Power Energy Syst.
[16] Kang Xiaoning, Suonan Jiale, Song Guobin, Bo ZQ. Protection technique based on parameter identification — its principle and application. In: 2008 IEEE power and energy society general meeting - conversion and delivery of electrical energy in the 21st century, Pittsburgh, PA. 2008, p. 1–6.
[17] Jia K, Li Y, et al. Transient current similarity based protection for wind farm transmission lines. Appl Energy 2018;225:42–51.
[18] Zheng L, Jia K, Bi T, Fang Y, Yang Z. Cosine similarity based line protection for large-scale wind farms. IEEE Trans Ind Electron 2021;68(7):5990–9.
[19] Jia K, Yang Z, Zheng L, Zhu Z, Bi T. Correlation-based protection for transmission line connected to wind farms, IEEE Trans Ind Informat.
[20] Banaiemoqadam A, Hooshyar A, Azzouz MA. A control-based solution for distance protection of lines connected to converter-interfaced sources during asymmetrical faults. IEEE Trans Power Deliv 2020;35(3):1455–66.
[21] Hooshyar A, Azzouz MA, El-Saadany EF. Distance protection of lines emanating from full-scale converter-interfaced renewable energy power plants—Part I: Problem statement. IEEE Trans Power Deliv 2015;30(4):1770–80.